EC Journals.ASM.org

Analysis of the *Aspergillus fumigatus* Biofilm Extracellular Matrix by Solid-State Nuclear Magnetic Resonance Spectroscopy

Courtney Reichhardt,[a] Jose A. G. Ferreira,[b,c]* Lydia-Marie Joubert,[d] Karl V. Clemons,[b,c] David A. Stevens,[b,c] Lynette Cegelski[a]

Department of Chemistry, Stanford University, Stanford, California, USA[a]; Department of Medicine, Division of Infectious Diseases and Geographic Medicine, Stanford University, Stanford, California, USA[b]; California Institute for Medical Research, San Jose, California, USA[c]; Cell Sciences Imaging Facility, Stanford University School of Medicine, Stanford, California, USA[d]

***Aspergillus fumigatus* is commonly responsible for lethal fungal infections among immunosuppressed individuals. *A. fumigatus* forms biofilm communities that are of increasing biomedical interest due to the association of biofilms with chronic infections and their increased resistance to antifungal agents and host immune factors. Understanding the composition of microbial biofilms and the extracellular matrix is important to understanding function and, ultimately, to developing strategies to inhibit biofilm formation. We implemented a solid-state nuclear magnetic resonance (NMR) approach to define compositional parameters of the *A. fumigatus* extracellular matrix (ECM) when biofilms are formed in RPMI 1640 nutrient medium. Whole biofilm and isolated matrix networks were also characterized by electron microscopy, and matrix proteins were identified through protein gel analysis. The ^{13}C NMR results defined and quantified the carbon contributions in the insoluble ECM, including carbonyls, aromatic carbons, polysaccharide carbons (anomeric and nonanomerics), aliphatics, etc. Additional ^{15}N and ^{31}P NMR spectra permitted more specific annotation of the carbon pools according to C-N and C-P couplings. Together these data show that the *A. fumigatus* ECM produced under these growth conditions contains approximately 40% protein, 43% polysaccharide, 3% aromatic-containing components, and up to 14% lipid. These fundamental chemical parameters are needed to consider the relationships between composition and function in the *A. fumigatus* ECM and will enable future comparisons with other organisms and with *A. fumigatus* grown under alternate conditions.**

Aspergillus fumigatus is the most important etiological agent of human aspergillosis and is recognized as a highly allergenic and opportunistic pathogen, causing acute and chronic infections particularly among immunocompromised individuals (1). Hospital-associated outbreaks of *A. fumigatus* may occur during periods of construction or renovation (2) or when fungi colonize water distribution systems that then lead to spore aerosolization in patient care areas and patient exposure (1). Additionally, *A. fumigatus* can cause infections as a result of colonizing medical implant devices, including cardiac pacemakers, joint replacements, and breast implants (3). Despite improvements in diagnostics and the antifungal armamentarium, including broad-spectrum azoles and the echinocandin antifungals, mortality due to *A. fumigatus* invasive infections remains high.

Like many microorganisms, *A. fumigatus* can also assemble into multicellular communities, termed biofilms, composed of cells plus an extracellular matrix (ECM) (4–9). Although more work is needed to fully understand the functional implications of biofilm formation by *A. fumigatus*, recent evidence suggests that the ECM may provide the infrastructure for enhancing cell density, controlling disaggregation, and altering nutritional needs, as well as providing a protective physical and chemical barrier that can decrease sensitivity to competitors and to antifungal drugs and the immune response (10). Understanding the composition of microbial biofilms and the ECM is important for considering functional differences among biofilm formers and, ultimately, for developing strategies to inhibit biofilm formation. Valuable detail has been obtained for many biofilms regarding macroscopic properties and the identification of key matrix parts (5, 7), but quantitative compositional detail remains sparse for most biofilm systems (11).

Mature *A. fumigatus* biofilms have been observed as three-dimensional assemblies between 10 μm and 200 μm thick. The putative parts list for the *A. fumigatus* ECM includes polysaccharides (galactomannon, galactosaminogalactan, α-1,3 glucans, and monosaccharides), proteins (major antigens and hydrophobins), melanin, and extracellular DNA (8). These identifications relied primarily upon immunoassays, yet suggested compositions vary depending upon the growth conditions and analysis methods. Attempts to generate quantitative descriptions of the *A. fumigatus* ECM have been limited to the soluble or low-molecular-weight components of the ECM. Indeed, the insoluble and complex nature of the ECM of most biofilms has posed a challenge to analysis by traditional techniques, which generally rely on dissolution of matrix parts and solution-based methods such as high-pressure liquid chromatography (HPLC)-mass spectrometry, protein analyses, and solution nuclear magnetic resonance (NMR) to examine soluble parts. Estimates of relative quantities of these components in the intact matrix are sometimes made. However, the

Received 17 March 2015 **Accepted** 6 July 2015

Accepted manuscript posted online 10 July 2015

Citation Reichhardt C, Ferreira JAG, Joubert L-M, Clemons KV, Stevens DA, Cegelski L. 2015. Analysis of the *Aspergillus fumigatus* biofilm extracellular matrix by solid-state nuclear magnetic resonance spectroscopy. Eukaryot Cell 14:1064–1072. doi:10.1128/EC.00050-15.

Address correspondence to Lynette Cegelski, cegelski@stanford.edu.

* Present address: Jose A. G. Ferreira, School of Medicine, Faculdade de Saúde e Ecologia Humana-FASEH, Vespasiano, Brazil.

C.R. and J.A.G.F. contributed equally to this article.

Supplemental material for this article may be found at http://dx.doi.org/10.1128/EC.00050-15.

inability to completely solubilize ECM components and the possible perturbations or degradation of material that can occur during sample preparation can severely compromise estimates of composition for the intact ECM. Thus, despite the prevalent roles that biofilms play in human infection, there has been little reliable quantitative information available regarding biofilm matrix composition.

Solid-state NMR spectroscopy is uniquely suited to study complex and insoluble biological materials (12) such as whole cells (13–18), biofilms, and the extracellular matrix (19–22). Solid-state NMR approaches can be used to quantify composition and to measure internuclear distances to determine parameters of architecture in such macromolecular assemblies and does not require soluble or crystalline samples (15). We recently introduced two approaches to define the composition of the insoluble ECM of bacterial biofilms using solid-state NMR integrated with complementary biochemical analysis and electron microscopy. Both approaches involve a panel of one-dimensional NMR experiments, which can be employed on any spectrometer equipped to perform solid-state NMR measurements. In the case of a uropathogenic *E. coli* biofilm that assembles an amyloid-associated ECM, we employed a bottom-up approach and discovered that the spectral addition of only two separate samples corresponding to separate isolated biofilm parts, (i) curli amyloid fibers and (ii) a modified form of cellulose, in a 6:1 ratio, was able to completely recapitulate the spectrum of the intact ECM (20). This was the first quantitative determination of the composition of an intact ECM preparation. In this approach, one requires separate samples of putative biofilm parts for analysis, and these are not readily available for many biofilm systems. Thus, while working with the more compositionally complex biofilms formed by *Vibrio cholerae*, we developed a top-down methodology that could be applied to other biofilm systems with only the complex ECM material to examine (21). In the top-down approach, carbon contributions are assigned by type of chemical functionality (e.g., carbonyls, aromatics, or anomerics) and quantified by peak integrals. If ^{15}N labeling of the growth medium is possible, then nitrogen pools can also be examined. In addition, the carbons can be more specifically annotated through ^{13}C-^{15}N recoupling experiments to determine, for example, what percentages of carbonyls may be part of peptide bonds versus non-nitrogen-bonded carbonyls. Together, the analysis of the *V. cholerae* biofilm formed on a minimal agar medium revealed a complex ECM dominated by highly modified polysaccharides, with additional contributions from lipids and proteins.

Here we provide our analysis of the biofilm composition of the filamentous fungus *A. fumigatus* grown in RPMI 1640 medium, a medium commonly employed for mammalian cell culture, using the top-down methodology that requires only the complex matrix material isolated from the hyphae. We integrated electron microscopy, protein gel and protein identification, and quantitative solid-state NMR measurements involving ^{13}C, ^{15}N, and ^{31}P nuclei to characterize the *A. fumigatus* biofilm. In order to permit ^{15}N NMR measurements, we generated a fully ^{15}N-labeled version of RPMI 1640 medium. Collectively, we provide a general spectral accounting of the carbon, nitrogen, and phosphorous contents and a detailed analysis of the carbon pools in the *A. fumigatus* ECM.

MATERIALS AND METHODS

***Aspergillus* growth and ECM extraction.** A standardized *Aspergillus fumigatus* suspension was inoculated in each of five 500-ml polystyrene tissue-culture flasks containing 100 ml of RPMI 1640 medium (final concentration of 10^5 conidia/ml) and incubated at 37°C for 96 h. To generate a fully ^{15}N-labeled version of RPMI 1640, all amino acids were replaced by 0.674 g/liter ^{15}N-labeled algal amino acid mixture (Aldrich, catalog number 608947). The algal extract contains between 65 and 95% amino acids by mass and has an isotope enrichment of 99% for ^{15}N. For uniformly ^{15}N-labeled samples, $Ca(NO_3)_2$ (98% ^{15}N enrichment) was also used in place of its unlabeled counterpart. Harvested biofilms were washed *in situ* twice with 100 ml of phosphate-buffered saline (PBS) to remove planktonic and loosely adherent cells. The sessile cells were then flooded with 40 ml of 10 mM Tris (pH 7.4) per flask and mixed mildly with a vortex mixer for 60 s. Each sample was transferred to a 50-ml conical tube and stored at 4°C until processing.

For the ECM extraction, the tubes containing the *A. fumigatus* biofilm were subjected to sonication (Fisher Scientific, model FB505; amplitude of 20%) for 10 min, followed by high-speed mixing on a vortex mixer for 30 s. The tubes were then centrifuged at 3,600 × *g* at 4°C for 15 min. The supernatant was poured into new tubes and centrifuged again to remove additional cells. The resulting supernatant was dialyzed against distilled water for 2 days (3.5-kDa molecular-mass cutoff). The supernatant was flash frozen in liquid nitrogen and lyophilized.

EM. Negative-staining transmission electron microscopy (TEM) was performed on ECM samples. Samples were applied to 300-mesh copper grids coated with Formvar film (Electron Microscopy Sciences, Hatfield, PA) for 2 min and then rinsed in deionized water. The samples were negatively stained with 2% aqueous uranyl acetate for 90 s, excess stain was wicked off with filter paper, and then the sample was air dried. Microscopy was performed with a JEM-1400 instrument (JEOL, LLC) operated at 120 kV. For scanning electron microscopy (SEM) analysis, *Aspergillus* biofilms were suspended in 10 mM Tris (pH 7.4), fixed for 45 min with 4% paraformaldehyde and 2% glutaraldehyde in 0.1 M sodium cacodylate buffer (pH 7.2), rinsed in the same buffer, and postfixed for 45 min with 1% aqueous OsO_4. After dehydration in an ascending ethanol series (50, 70, 90, and 100% [twice]; 5 min each), samples were gently vacuum filtered onto 0.2- and 0.45-μm polyamide filters (Sartorius, Bohemia, NY) kept under a steady stream of 100% ethanol. Samples were then critical-point dried with liquid CO_2 in a Tousimis Autosamdri-815B apparatus (Tousimis, Rockville, MD), mounted onto double-sided copper tape on 15-mm aluminum stubs (Electron Microscopy Sciences, Hatfield, PA), and sputter coated with 50 Å of gold-palladium using a Denton Desk II sputter coater (Denton Vacuum, Moorestown, NJ). Visualization was performed both with a Hitachi S-3400N SEM (Hitachi HTA, Dallas, TX) operated at 10 to 15 kV using Everhart Thornley secondary electron (SE) detection and with a Zeiss Sigma field emission SEM (FESEM) (Carl Zeiss Microscopy, Thornwood, NY) operated at 2 kV using InLens SE detection at a working distance of 4 to 5 mm. Images were captured in TIFF using store resolution of 2,048 by 1,536 and a line averaging noise reduction algorithm.

SDS-PAGE protein analysis and identification. Lyophilized ECM was suspended in SDS-PAGE sample buffer containing 8 M urea and 50 mM dithiothreitol (DTT) and used for electrophoresis in a 4 to 20% gradient Tris-glycine SDS-polyacrylamide gel (Novex). For Edman degradation (UC Davis Proteomic Core), samples were transferred to a polyvinylidene difluoride (PVDF) membrane and were loaded onto an ABI Procise sequencer and subjected to Edman degradation. In this processing, for each residue/cycle, the free N terminus of each immobilized protein was coupled with phenyl isothiocyanate, cleaved with trifluoroacetic acid, and then converted to the more stable phenylthiohydantion amino acid derivative, which was separated by reverse-phase chromatography and detected by UV-visible spectrophotometry.

Solid-state NMR. All solid-state NMR experiments were performed using an 89-mm wide-bore Varian magnet at 11.7 T (499.12 MHz for ^{1}H,

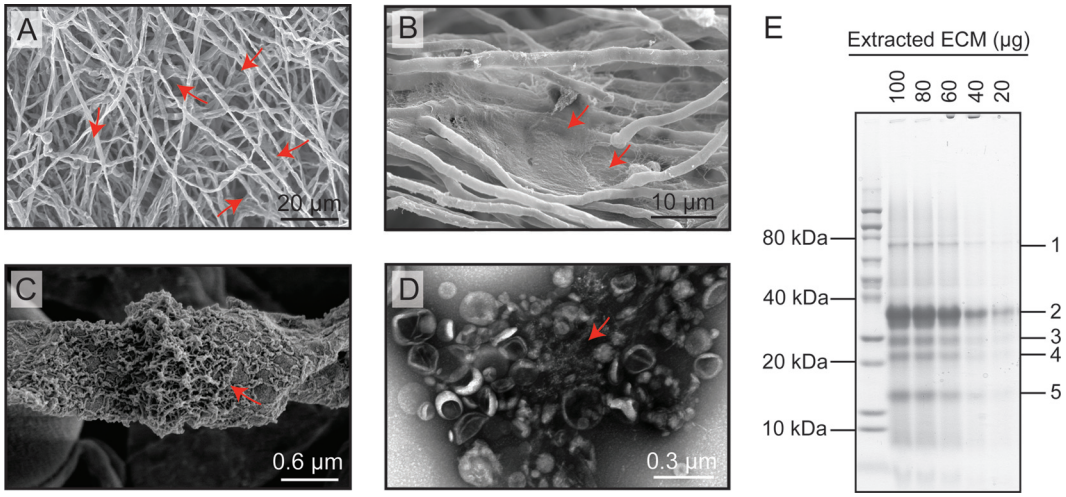

FIG 1 Electron microscopy of *A. fumigatus* biofilm preparations and ECM protein analysis. (A to C) Scanning electron micrographs of intact *A. fumigatus* biofilm. (A) This lower-magnification micrograph shows the collection of hyphae associated with the *A. fumigatus* biofilm formed in the modified version of RPMI medium used in this study. ECM connective material is present between some of the hyphae (indicated by red arrows). (B) At higher magnification, wide sheets of ECM are seen stretching between hyphae. (C) ECM that is closely associated with hyphae can be observed at the highest resolution, with an apparent rough and web-like coating. (D) Transmission electron micrograph of isolated *A. fumigatus* ECM. Fibrous material is indicated by a red arrow, and vesicle-type structures are also apparent. (E) SDS-PAGE protein gel of the *A. fumigatus* ECM. Five representative bands of the SDS-soluble proteins (labeled 1 to 5) were excised and identified. Catalase B (band 1, 79,910 Da) and Asp f2 (band 2, 32, 838 Da) were specifically identified. Bands 3 to 5 corresponded to processed forms of these two proteins.

125.52 MHz for ^{13}C, and 50.58 MHz for ^{15}N) and an 89-mm wide-bore Agilent magnet at 11.7 T (500.92 MHz for ^{1}H, 125.97 MHz for ^{13}C, 50.76 MHz for ^{15}N, and 202.78 MHz for ^{31}P), Varian/Agilent consoles, and home-built four-frequency transmission line probes with a 13.66-mm-long, 6-mm-inner-diameter sample coil and a Revolution NMR magic-angle spinning (MAS) Vespel stator. Samples were spun in thin-wall 5-mm-outer-diameter zirconia rotors (Revolution NMR, LLC) at 7,143 ± 2 Hz, using a Varian MAS control unit. The temperature was maintained at −10°C. For all NMR experiments, π pulse lengths were 7 μs for ^{1}H and 10 μs for ^{13}C, ^{15}N, and ^{31}P. Proton-carbon and proton-nitrogen cross-polarization occurred at 50 kHz for 1.5 ms unless otherwise noted. Proton dipolar coupling was performed at 90 kHz with two-pulse phase modulation (TPPM). For all experiments, the recycle delay was 2 s. The ^{13}C spectra were referenced to tetramethylsilane (TMS), ^{15}N spectra were referenced to liquid ammonia, and ^{31}P spectra were referenced to phosphoric acid. All chemical shift references were determined relative to an adamantane standard. Rotational-echo double-resonance (REDOR) dephasing was calculated using peak integral values. Multipeak fitting and integration were performed in software written for Igor Pro (WaveMetrics, Lake Oswego, OR, USA).

RESULTS

***A. fumigatus* biofilm formation and ECM isolation and protein analysis.** A biofilm contains both microbial cells and their secreted extracellular matrix (ECM) (23). The *A. fumigatus* biofilm was visualized by scanning electron microscopy (SEM) (Fig. 1A to C). The biofilm hyphae are densely packed and connected to one another by tightly woven webs of ECM. The ECM also appears as fibrous and granular networks coating the individual hyphae (Fig. 1C). The biofilms are similar in appearance to the *A. fumigatus* biofilms grown in aerial static cultures, as reported by Beauvais et al. (5), with some ECM material covering individual hyphae and some serving to glue hyphae together into a contiguous network. To examine the ECM separately from the hyphae, we developed a minimally perturbative ECM extraction protocol that included sonication to disrupt the biofilm and subsequent centrifugation to separate the hyphae from the ECM. The extracted ECM was best imaged by transmission electron microscopy (TEM), which revealed aggregative material, including fibrous strands and vesicle-type structures (Fig. 1D). SDS-PAGE analysis of the ECM yielded bands corresponding to several SDS-soluble proteins of different molecular weights (Fig. 1C). Gel bands corresponding to the proteins that were in relatively high abundance were excised and analyzed by mass spectrometry and Edman sequencing for protein identification. Although proteins may escape detection by PAGE analysis if they are not soluble and not able to run into the gel, this analysis at least allowed for the identification of the proteins that could be detected to help characterize the ECM preparation and to be sure that cellular contaminants were not associated with the preparation. Two unique proteins, catalase B and Asp f2 (major allergen), were identified by mass spectrometry and by Edman degradation and have molecular masses of 79,910 Da (band 1, catalase B) and 32,838 Da (band 2, Asp f2). Importantly, both proteins are typically secreted from cells and found at or beyond the cell surface of *A. fumigatus* (24–26). Both proteins are N-linked glycosylated, and digestion with peptide-*N*-glycosidase F (PNGase) enhanced the intensity of band 3 while depleting band 2 intensity (see Fig. S1 in the supplemental material). By Edman degradation, the protein in band 3 also contained the same N-terminal amino acids as Asp f2. Thus, band 3 represents deglycosylated Asp f2. Band 4 is a truncated form of catalase B, with the N terminus corresponding to residue 334 from the full-length protein sequence (determined by Edman degradation analysis). The protein in band 5 appears to be Asp f2, containing the same N terminus as full-length Asp f2. It may appear at a lower apparent molecular weight due to an altered glycosylation pattern, or it may have a truncated C terminus.

Spectral comparisons of intact *A. fumigatus* biofilms (cells plus matrix) and the isolated ECM. To obtain quantitative detail on the *A. fumigatus* ECM composition, we employed a top-down

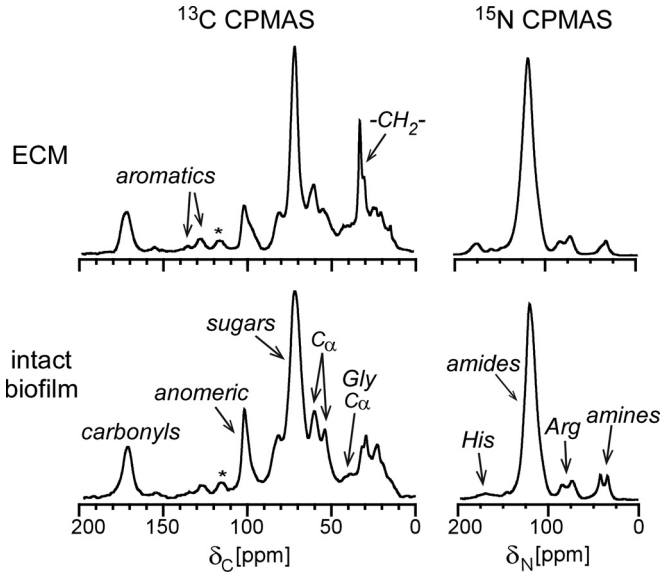

FIG 2 Spectral comparisons of the carbon and nitrogen composition of the *A. fumigatus* biofilm and isolated ECM. The ^{13}C CPMAS spectrum of the *A. fumigatus* intact biofilm sample (cells plus ECM) contains major contributions from polysaccharides, consistent with the thick hyphal cell walls (45,000 scans). The ^{13}C CPMAS spectrum of the ECM is consistent with a material containing proteins (carbonyl and alpha carbon peaks), aromatic compounds (such as melanin), and polysaccharides (48,000 scans). The spinning side bands, which are a result of the magic-angle spinning and not representative of a specific carbon type, are indicated by asterisks. The ^{15}N CPMAS spectrum of the whole biofilm contains a prominent peak centered at 122 ppm that is indicative of amides. The smaller peaks are indicative of nitrogen-containing amino acid side chains (12,000 scans). The ^{15}N CPMAS spectrum of the ECM contains a similarly prominent amide peak centered at 119 ppm plus other smaller peaks and nitrogen contributions (12,000 scans).

solid-state NMR approach, as described in the introduction, which does not depend upon sample solubility or crystallinity. A standard way to obtain a carbon spectrum by solid-state NMR spectroscopy is through cross-polarization magic-angle spinning (CPMAS), introduced in 1976 (27, 28). During CPMAS, carbon magnetization is enhanced through spin polarization contact with an abundant ^{1}H spin lattice, which is present in nearly all biomaterials (28), and the sample is mechanically spun at the magic angle to help suppress dipolar couplings and chemical shift anisotropy that would broaden the resonances significantly. The ^{13}C CPMAS spectrum of the intact *A. fumigatus* biofilm containing hyphae plus associated ECM has strong polysaccharide peaks (anomerics, 100 to 105 ppm; ring-sugar carbons, 60 to 85 ppm), consistent with the presence of chitin and additional polysaccharides associated with the thick hyphal cell walls (Fig. 2) (7, 29, 30). The ^{13}C CPMAS spectrum of the extracted ECM reveals a different profile of carbon pools reflective of its composition. The ECM spectrum contains carbon chemical shifts that are representative of proteins (carbonyl, 173 ppm; α-carbons, 50 to 60 ppm; glycine α-carbons, 38 to 43 ppm), other aliphatics (10 to 35 ppm), polysaccharides (anomeric carbons, 97 to 103 ppm; ring sugar carbons, 60 to 85 ppm), lipids (24, 33, and 173 ppm), and aromatic compounds (130 to 160 ppm) (Fig. 2). Relative intensities differ between the intact biofilm and ECM spectra. In addition, the polysaccharide peaks of the ECM sample exhibit a slight upfield shift with respect to those of the biofilm sample, indicative of a difference in carbohydrate composition or local chemical environment. The differences between the spectra of the biofilm and extracted ECM, together with the protein gel and EM characterization of the ECM, suggest that the ECM extraction resulted in a material free of hyphal contamination.

To use peak integrals or peak heights from CPMAS spectra quantitatively, one must account for the possibility that some carbons might exhibit differences in cross-polarization efficiency or relaxation. Thus, CPMAS spectra were obtained as a function of CP time, where normalized intensities could be obtained based on possible differences due to CP (see Fig. S2 in the supplemental material). Nearly all carbons exhibited similar CP behavior, with differences noted in some aliphatic carbons. The polysaccharide anomeric carbons and associated ring sugar carbons are a prominent spectral feature and account for approximately 43% of the total carbon mass. The relative contributions of other spectral regions within the ^{13}C spectrum, after all the carbon pools were first more fully annotated using additional NMR measurements described below, are fully outlined in Table 1.

To assess possible compositional variation between different biofilm samples and ECM extractions, we collected ^{13}C CPMAS spectra of two separately cultured biofilm samples and their corresponding identically prepared ECM samples (Fig. 3). The major differences between samples obtained from the two separate cultures occur in peaks uniquely attributed to polysaccharides, and changes in overall polysaccharide content in the intact biofilms were similarly present in the corresponding extracted ECM preparations. As anticipated, ECM extracted from biofilms with high overall polysaccharide content also had greater polysaccharide content. In the ECM samples, the percentage of carbon that is attributed to polysaccharide ranges from 20 to 43% of the total carbon mass. Therefore, differences in ECM composition could be attributed to biological variability in biofilm production and not necessarily to differences in ECM extraction. The fact that the polysaccharide carbons increase without associated increases in carbonyls or α-carbons indicates that these polysaccharides are not significantly modified, unlike the more complex *Vibrio* polysaccharide (VPS), which contains extensive acetyl and glycine modifications (21). The observed variability in the *A. fumigatus* ECM polysaccharide content is in contrast to what we have previously observed for *Escherichia coli* ECM, which maintains a nearly constant protein-to-polysaccharide ratio of 6:1 for samples grown in the same way (20). Thus, we speculate that there may be more flexibility in the range of polysaccharide required to permit biofilm formation in biofilms with relatively high polysaccharide content. All subsequent NMR experiments and analyses were performed on the biofilm and corresponding ECM samples with greater polysaccharide content.

The ^{15}N CPMAS spectrum of *A. fumigatus* biofilm contains a prominent peak centered at 122 ppm as well as peaks corresponding to multiple amine types and amino acid side chains (Fig. 2). In contrast, the ^{15}N CPMAS spectrum of the ECM contains a single prominent amide signal centered at 119 ppm, which is upfield of the amide peak in the biofilm spectrum, encompassing 90% of the total integrated spectral area (Fig. 2). The quantitative ^{15}N spectral contributions were also determined by analysis of CPMAS spectra obtained as a function of CP time (see Fig. S3 in the supplemental material). Amides are present in all peptides and some amino acid side chains and can be present as modifications among other biomolecules, e.g., N-acetyl modifications. The ^{15}N peaks at 34

TABLE 1 Defined carbon pools in the *A. fumigatus* ECM (grown in modified RPMI medium)

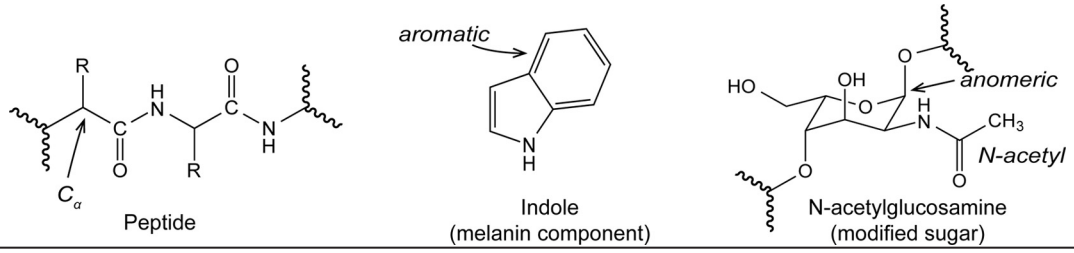

Chemical shift, ^{13}C (ppm)	Carbon type	Carbon mass (% of total)	Molecules
173	Carbonyls	12	Amino acids, phospholipids, N- and O-acetyl modifications
130–160	Aromatics	3	Melanin, amino acids
94–104	Anomerics	8[a]	Sugars
60–80	Ring carbons	35[a]	Sugars
50–60	Other C_α	7	Amino acids
38–43	Gly C_α	0.30	Gly
33	CH_2s	10	Amino acids, fatty acid chains
12–25	Methyls	18	Acetyl groups, amino acids

[a] Values are provided for the first sample based on the full analysis in this paper. The notable difference in a second ECM sample is the reduced polysaccharide content with 4% anomeric carbons and 15% ring carbons.

and 40 ppm correspond to amines, such as those present in the side chain of lysine and those present as amino modifications of other biomolecules. Together, the amines in the ECM account for 4% of the nitrogen spectral area. The ^{15}N peaks at 73 and 84 ppm correspond to the side chain nitrogens of arginine and together account for 4% of the spectral area of the ECM. The spectrum also contains a peak at 174 ppm, where imidazole nitrogens in histidine side chains would appear, and accounts for 2% of the ECM spectrum.

Detailed analysis of the *A. fumigatus* ECM carbon pools using $^{13}C\{^{15}N\}$REDOR NMR. Protein carbonyls and α-carbon chemical shifts appear at 173 and 50 to 60 ppm, respectively. How-

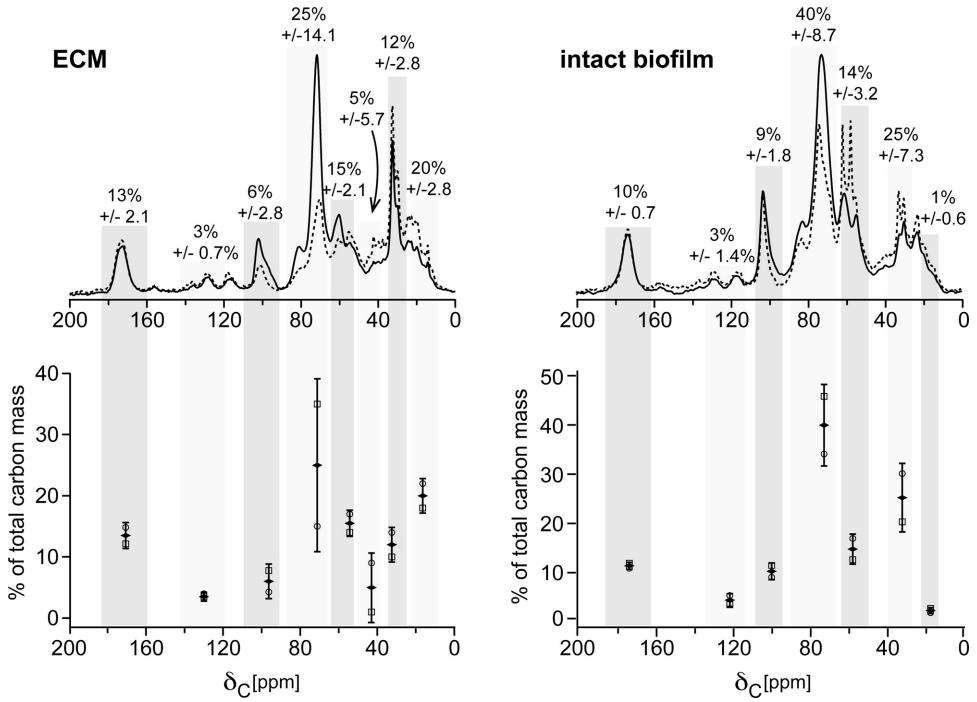

FIG 3 Two-sample comparison of ECM carbon contributions. ^{13}C CPMAS spectra of two ECM samples revealed variations in the polysaccharide content. Analysis of the ECM samples (left) isolated from their corresponding biofilms (right) identified differences in peaks uniquely attributed to polysaccharides. The solid-line spectra are from Fig. 2 and are shown for direct comparison with the dashed-line spectra from a second sample. The percentage of carbon attributed to polysaccharide in the isolated ECM samples ranges from 20 to 43% of the total carbon mass. The error bars represent the standard deviation. Corresponding differences were observed in the intact biofilm. Carbon mass percentages in the ECM were determined by quantitative CPMAS, performing CPMAS as a function of CP time for extrapolation. The intact biofilm analysis is based on the CPMAS spectra shown.

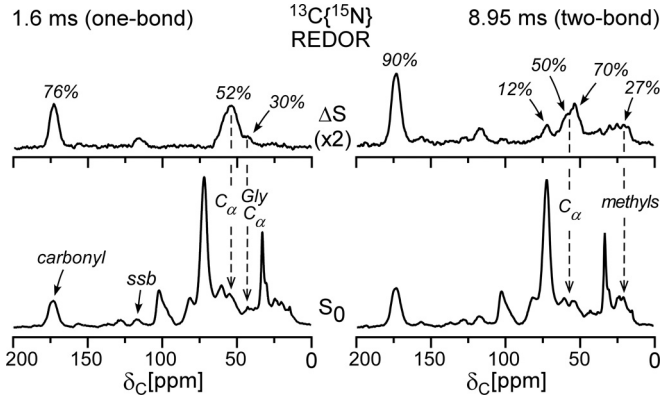

FIG 4 Spectroscopic selection of one-bond and two-bond C-N pairs. $^{13}C\{^{15}N\}$REDOR with a 1.6-ms evolution time identified carbons, and the percentage of those carbons, that are directly bonded to a nitrogen (64,000 scans for both S_0 and S). $^{13}C\{^{15}N\}$REDOR performed with an evolution time of 8.95 ms revealed carbons that were within a two-bond proximity to nitrogen (43,760 scans for both S_0 and S spectra).

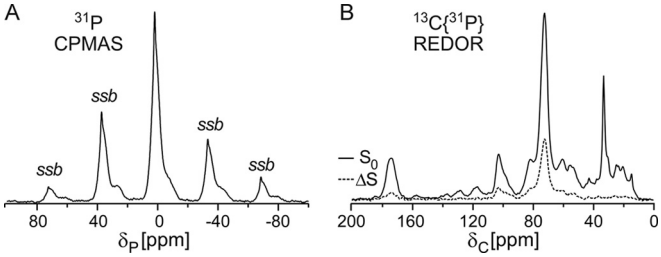

FIG 5 Phosphorus contributions to the ECM. (A) ^{31}P CPMAS analysis of *A. fumigatus* ECM. The ^{31}P CPMAS spectrum exhibited three overlapping chemical shifts and their associated spinning sidebands, as indicted by *ssb* (9,168 scans). (B) Spectroscopic selection of carbons near to phosphorous. $^{13}C\{^{31}P\}$REDOR was performed with an evolution time of 8.95 ms. The REDOR difference spectrum (ΔS, dashed spectrum) reveals the few carbon types that are proximate to ^{31}P (38,000 scans for both S_0 and S spectra).

ever, carbons from other biomolecular groups may also contribute to these spectral regions. Proteins contain amino acids with α-carbons and carbonyls that are each directly bonded to nitrogen, and based upon the uniqueness of these carbon-nitrogen pairs, we are able to spectroscopically select and determine the relative amounts of nitrogen-bonded carbonyls and α-carbons within a carbon spectrum of a complex material. To quantify the relative contribution of proteins to the ECM, we employed $^{13}C\{^{15}N\}$REDOR with 1.6-ms dephasing to select directly bonded ^{13}C-^{15}N pairs (Fig. 4, left). REDOR experiments are done in two parts: one reference spectrum is collected without dephasing pulses (S_0), and one "dephased" spectrum is collected with rotor-synchronized dephasing pulses (S) to reintroduce the dipolar couplings that are suppressed during magic-angle spinning (31). The difference spectrum (ΔS) is obtained from the subtraction of the S spectrum from the S_0 spectrum. Only carbons that are proximate to the dephasing spin contribute to intensities in the ΔS spectrum. In the case of $^{13}C\{^{15}N\}$REDOR with 1.6-ms dephasing, the ΔS spectrum reports on those carbons directly bonded to nitrogen. At longer dephasing times, one can extend this ruler to examine longer-range C-N contacts.

In the ^{13}C CPMAS spectrum of *A. fumigatus* ECM, the carbonyl peak accounts for 12% of the carbon, and it exhibited 76% dephasing in the one-bond $^{13}C\{^{15}N\}$REDOR measurement. Thus, at most, only 76% of all carbonyl carbons are directly bonded to nitrogen, which indicates that 9% of the total ^{13}C CPMAS spectral area can be assigned to nitrogen-bonded carbonyls (76% of 12%). Carbonyl-nitrogen pairs occur in peptide bonds of proteins as well as in N-acetyl groups. Glycine α-carbons appear near 40 ppm, while all the other α-carbons contribute to the resonances centered at 55 and 60 ppm. Other chemical species can also contribute to these spectral regions, and examples include the C-6 carbons of hexose-based polysaccharides. Thus, the REDOR measurement is used to quantify the percentage of these carbons that are adjacent to a nitrogen and thus can be attributed to α-carbons. The integrals of the resonances at 55 and 60 ppm together account for 14% of the total ^{13}C CPMAS spectral area (Fig. 2), and the region exhibited 52% dephasing. Thus, we can place an upper limit on the carbon mass that can be attributed to protein α-carbons as 7% (52% of 14%). The region near 40 ppm exhibited 30% dephasing, suggesting that 0.3% of the total carbon mass is due to glycyl α-carbons. The approximate 1:1 ratio of the numbers of nitrogen-bonded carbonyls (9%) to α-carbons (7%) is consistent with that expected for protein, and the 1:23 ratio of glycine α-carbons (0.3%) to other α-carbons (7%) is also within expectations for the composition of average proteins. The slight 2% excess of nitrogen-bonded carbonyls relative to α-carbons would be consistent with the presence of nitrogen-bonded carbonyls in N-acetyl modifications.

The extent to which carbons were within a longer, approximately 2.5-Å proximity to a nitrogen was examined using $^{13}C\{^{15}N\}$REDOR with an evolution time of 8.95 ms (Fig. 4, right). As expected, the carbonyl and α-carbon regions exhibited additional dephasing. The CH_2 region centered at 33 ppm accounts for 10% of the total carbon spectral area and exhibits 16% dephasing. The CH_2 carbons that are spatially close to nitrogen encompass 2% (16% of 10%) of all carbons and can be accounted for by amino acid side chains, especially those that also contain side chain nitrogen, including arginine, glutamine, and lysine. The remaining intensity at 33 ppm can be attributed to the aliphatic CH_2 groups of lipids and accounts for 8% of the total carbon mass. Dephasing in the aliphatic regions (12 to 35 ppm) also was observed, indicative of the presence of amino acid side chains and possible N-acetyl modifications. The 12- to 25-ppm region, which includes methyl groups such as those in amino acids, acetyl modifications, and termini of fatty acids, constitutes 18% of the total ^{13}C CPMAS spectral area and exhibits 27% dephasing, suggesting that 5% (27% of 18%) of carbons belong to side chains of amino acids such as alanine or exist as methyl groups of N-acetyl modifications. The observed 12% dephasing of the 72-ppm sugar peak further supports the presence of N-acetyl modifications of polysaccharides such those in galactosaminogalactan (4), which was previously shown to be a component of the *A. fumigatus* ECM, or in the *N*-acetylglucosamine (GlcNAc) moieties involved in N-linked glycosylation of some *A. fumigatus* extracellular proteins.

^{13}C-^{31}P couplings indicate the presence of phosphorus-containing biomolecules in the ECM. To examine the possibility that phosphorus-containing biomolecules contribute to *A. fumigatus* ECM, we performed ^{31}P NMR experiments. The ECM ^{31}P CPMAS spectrum (Fig. 5A) contained a broad resonance that could be fit by three peaks centered at −7, −0.4, and 2 ppm (see Fig. S4 in the supplemental material), with the corresponding side

bands separated by the MAS frequency. These ^{31}P shifts could be due to a multitude of phosphorylated biomolecules, including lipids, proteins, sugars, or nucleic acids. To better evaluate possible origins of phosphorous contributions to the ECM, we performed ^{13}C{^{31}P}REDOR with 8.95-ms dephasing to identify any carbons that were proximate to phosphorous (Fig. 5B). With this one long-range REDOR evolution time, the measurement serves as a qualitative analysis that could identify the presence of a few C-P contacts in close proximity (within 6 Å) or many C-P contacts at longer range (>6 Å). We observed dephasing by phosphorous of the carbon peaks centered at 60, 72, and 80 ppm as well as the carbonyl peak at 173 ppm (Fig. 5B, dashed REDOR difference spectrum [ΔS]). Biomolecules that contain phosphorus atoms that are spatially close to carbons with chemical shifts near 60 to 80 ppm include nucleic acids (phosphorylated ribose), phospholipids, phosphorylated sugars, and proteins that are phosphorylated on serine or threonine residues. The dephasing of the carbonyl peak by phosphorus is consistent with phospholipid and phosphorylated proteins (21, 32). If the only phosphorus-containing molecules in the ECM were phospholipids, we would have observed dephasing of the 33-ppm peak corresponding to lipid aliphatics. Similarly, phosphorylated proteins could account for only a fraction of the total ^{13}C{^{31}P}REDOR ΔS spectrum, even if every threonine and serine in the identified ECM proteins, catalase B and Asp f2, was phosphorylated. Thus, it is possible that multiple types of biomolecules contribute to the phosphorus pools of *A. fumigatus* ECM.

DISCUSSION

Our integrated solid-state NMR, electron microscopy, and biochemical analyses of the composition of the *A. fumigatus* ECM extracted from cells grown in RPMI 1640 medium provide insight into the identification and contributions of biomolecules present in the ECM. Electron micrographs of the *A. fumigatus* biofilm revealed sheets of ECM that connected some, but not all, of the hyphae in the dense community of cells (Fig. 1). The ECM also served to coat some of the hyphae, giving them a rough and granular web-like appearance. Inspection by electron microscopy is invaluable in revealing biofilm architecture and in characterizing the extracted ECM but does not provide insight into chemical and molecular composition. The ^{13}C NMR results defined the quantities of carbon types, including carbonyls, aromatic carbons, polysaccharide carbons (anomeric and nonanomerics), and aliphatics, present in the insoluble ECM material. The ^{15}N and ^{31}P NMR spectra provided additional detail regarding nitrogen and phosphorous pools in the ECM. Furthermore, by ensuring full incorporation of ^{15}N labels into the sample, we were able to further refine and quantify specific types of carbons, including one-bond C-N pairs, such as those in peptide carbons and alpha carbons. The full definition of the carbon pools is summarized in Table 1 and provides the absolute atomic-level parameters of the ECM obtained directly from the NMR measurements. Assimilating these data as discussed further below, we find that the *A. fumigatus* ECM at the molecular level contains approximately 40% protein, 43% polysaccharide, 3% aromatic-containing components, and at least 8% lipid. Additionally, we identified the presence of phosphorus-containing biomolecules in the ECM, although we did not specifically annotate them in this study.

Polysaccharides (anomerics and ring sugars) account for approximately 43% of the total ECM carbon mass (Fig. 2 and Table 1; see Fig. S2 in the supplemental material), although variability in polysaccharide content between separate cultures was observed (Fig. 3) and a second sample was reduced in its polysaccharide content (with sugar carbons representing 20% of the carbon mass). Thus, biologically, the *A. fumigatus* ECM exhibits variation in the range of polysaccharide production during biofilm formation under comparable conditions. This is unlike the case for *E. coli*, where under given growth conditions, the insoluble ECM composition exhibits very little variability (85 to 87% curli protein and 13 to 15% modified cellulose). The *A. fumigatus* NMR results are consistent with polysaccharides previously reported to be present in *A. fumigatus* biofilm, which include galactomannan, galactosaminogalactan, α-1,3 glucans, and monosaccharides. Galactosaminogalactan, which is a polymer of galactose and *N*-acetylglucosamine, plays a critical role in the adherence and virulence of *A. fumigatus* (33), and the presence of N-acetyl modifications, such as occur in galactosaminogalactan, was supported by the ^{13}C{^{15}N}REDOR analyses.

Protein accounts for approximately 40% of the total ECM carbon mass. This estimation stems from the absolute NMR determination that amino acid α-carbons and nitrogen-bonded carbonyls account for 7% and 9% of the carbon mass, respectively. Amino acids contain an average of 5.4 carbons, and thus, three additional carbons, on average, can be attributed to protein and would contribute broadly to the aliphatic spectral region, consistent with what is observed (Fig. 2). In addition, the ^{15}N CPMAS (Fig. 2) spectrum and the ^{13}C{^{15}N}REDOR results (Fig. 4) suggest that most nitrogen is present in protein and that there is very little nitrogen that exists as modifications to other biomolecules.

Protein gel analysis identified catalase B and Asp f2 as the major proteins in the ECM. Asp f2 has been associated with damage to the host epithelium and host inflammatory reactions during fungal colonization (26). Accumulation of catalase B in the ECM of *A. fumigatus* biofilms has been detected by immunolabeling assays (5, 34), and catalase is reported to play a critical role in other microbial biofilms, including those formed by *Pseudomonas aeruginosa* (35). The presence of catalase B in the ECM is also consistent with its protective role against reactive oxygen species, specifically hydrogen peroxide, which microbes may encounter during infection of a host. Increased catalase production generally reduces the susceptibility of microorganisms to phagocytosis and killing (36, 37). It was previously reported that the *A. fumigatus* ECM contained 2% (wt/wt) protein, which was determined using the colorimetric Bradford assay (5). We similarly performed a bicinchoninic acid (BCA) protein assay to determine protein concentration. Using this colorimetric assay, we found the ECM to contain an apparent estimate of 18% (wt/wt) protein. We know from the NMR results that this value is an underestimate of the protein concentration and is likely due to inaccessibility of protein peptide bonds within the matrix to reduce Cu^{2+} ions in the BCA assay or due to complexation of Cu^{2+} by other components. This finding provides another example of how solution-based methods, particularly such chemical reaction assays used for proteins within a complex mixture, can fail to quantify composition in intact and insoluble materials such as the *A. fumigatus* ECM.

For the final accounting, according to carbon mass, an additional 3% of the carbon mass was attributed to aromatic molecules such as melanin (130 to 160 ppm). The presence of melanin in *A. fumigatus* and other fungi is considered to be important for viru-

lence because it affects the immune response to fungal infection (38). We observe some dephasing in the aromatic carbon region in the $^{13}C\{^{15}N\}$REDOR experiments that is consistent with melanin (example structure in Table 1) (39, 40), but due to the overlap of ^{15}N chemical shifts of amides and indoles (near 120 ppm) in the ^{15}N spectrum, it is not possible to unambiguously identify whether the indole nitrogens are specifically attributed to melanin. The remaining 14% of the ^{13}C CPMAS spectral area contains additional carbonyls (excluding nitrogen-bonded carbonyls already accounted for) and aliphatics, with the presence of sharp CH_2 peaks, consistent with lipid molecules. Thus, the ECM contains at least 8% lipid due to aliphatic CH_2 groups and up to 14% lipid in total. The carbonyl dephasing by phosphorous in the $^{13}C\{^{31}P\}$REDOR experiment (Fig. 5) also suggests that *A. fumigatus* ECM contains some phospholipids. There is no evidence for a prominent contribution from nucleic acids in the *A. fumigatus* ECM characterized here, as the ^{13}C CPMAS spectrum contains minimal contributions to aromatic regions and the ^{15}N spectrum lacks peaks corresponding to nucleic acid ^{15}N chemical shifts. It is possible that this lack of nucleic acids is due to the age of the biofilm when harvested and that older, more mature biofilms would have nucleic acids present in higher concentration. The lack of nucleic acids in our samples also indicates that the fungal biofilm is not necessarily dependent on nucleic acids for structural integrity, as electron microscopy revealed the anticipated elaboration of ECM around and between the hyphae (41).

Thus, we determined the ECM composition of *A. fumigatus* to be approximately 40% protein, 43% polysaccharide, 3% aromatic compounds such as melanin, and up to 14% lipid. The ECM composition of *A. fumigatus* can be richer in polysaccharides than the ECM composition reported for *Candida albicans*, with 55% protein, 25% carbohydrate, 15% lipid, and 5% nucleic acid (24). The analysis of the *Candida albicans* matrix material, however, used different chemical and solution-based methods to estimate matrix parts. Carbohydrate content was determined colorimetrically using a phenol-sulfuric acid precipitation protocol, protein concentration was determined using a BCA assay, lipids were extracted in organic solvent and analyzed by HPLC-mass spectrometry, and nucleic acid concentration was estimated by absorbance at 260 nm. Mass spectrometry, in particular, is invaluable in the specific identification of matrix components, but the overall modeling of the intact matrix composition and quantification from the analysis of soluble parts are limited. Our top-down NMR approach to characterize the ECM composition enables quantitative analysis. The NMR approach required only preparation of a uniformly ^{15}N-labeled *A. fumigatus* sample with extraction of the ECM and no harsh hydrolyses, degradative measures, or caveats associated with attempting to quantify parts using solution-based assays that are subject to sampling bias and errors. Protein gel analysis provides a qualitative evaluation of the relative quality of the ECM preparation (detecting no contaminating intracellular proteins) and can identify the proteins in the ECM that are soluble and can be accessed and compared among samples, for example. The NMR analysis should also be coupled with microscopy to provide visual inspection of the biofilm and ECM.

In summary, our analyses provide fundamental atomic-level compositional parameters in the complex ECM needed to consider the relationship between composition and function in the *A. fumigatus* ECM. Future comparisons with the ECM analysis of *A. fumigatus* under other growth conditions and with ECM from other strains will enable us to further build such composition-function relationships.

ACKNOWLEDGMENTS

This research was supported in part by the NIH Director's New Innovator Award to L.C. (DP2OD007488). We also acknowledge funding from the Child Health Research Institute, Stanford Transdisciplinary Initiatives Program (D.A.S.), and a gift from John Flatley (D.A.S.). C.R. is supported by the Althouse Stanford Graduate Fellowship, and J.A.F. has been partially supported by the Programa Ciencias sem Fronteiras CsF/CNPq (Brazilian National Research Council). We acknowledge support from the Cell Sciences Imaging Facility at Stanford (NIH grant 1S10RR02678001) for electron microscopy access.

REFERENCES

1. **Latge JP.** 2001. The pathobiology of *Aspergillus fumigatus*. Trends Microbiol **9:**382–389. http://dx.doi.org/10.1016/S0966-842X(01)02104-7.
2. **Haiduven D.** 2009. Nosocomial aspergillosis and building construction. Med Mycol **47:**S210–216. http://dx.doi.org/10.1080/13693780802247694.
3. **Rosenblatt WB, Pollock A.** 1997. *Aspergillus flavus* cultured from a saline-filled implant. Plast Reconstr Surg **99:**1470–1472.
4. **Muller F-MC, Seidler M, Beauvais A.** 2011. *Aspergillus fumigatus* in the clinical setting. Med Mycol **49:**S96–S100. http://dx.doi.org/10.3109/13693786.2010.502190.
5. **Beauvais A, Schmidt C, Guadagnini S, Roux P, Perret E, Henry C, Paris S, Mallet A, Prevost MC, Latge JP.** 2007. An extracellular matrix glues together the aerial-grown hyphae of *Aspergillus fumigatus*. Cell Microbiol **9:**1588–1600. http://dx.doi.org/10.1111/j.1462-5822.2007.00895.x.
6. **Beauvais A, Loussert C, Prevost MC, Verstrepen K, Latge JP.** 2009. Characterization of a biofilm-like extracellular matrix in FLO1-expressing *Saccharomyces cerevisiae* cells. FEMS Yeast Res **9:**411–419. http://dx.doi.org/10.1111/j.1567-1364.2009.00482.x.
7. **Beauvais A, Fontaine T, Aimanianda V, Latge JP.** 2014. *Aspergillus* cell wall and biofilm. Mycopathologia **178:**371–377. http://dx.doi.org/10.1007/s11046-014-9766-0.
8. **Kaur S, Singh S.** 2014. Biofilm formation by *Aspergillus fumigatus*. Med Mycol **52:**2–9. http://dx.doi.org/10.3109/13693786.2013.819592.
9. **Mowat E, Butcher J, Lang S, Williams C, Ramage G.** 2007. Development of a simple model for studying the effects of antifungal agents on multicellular communities of *Aspergillus fumigatus*. J Med Microbiol **56:**1205–1212. http://dx.doi.org/10.1099/jmm.0.47247-0.
10. **Manavathu EK, Vager DL, Vazquez JA.** 2014. Development and antimicrobial susceptibility studies of in vitro monomicrobial and polymicrobial biofilm models with *Aspergillus fumigatus* and *Psuedomonas aeruginosa*. BMC Microbiol **14:**53. http://dx.doi.org/10.1186/1471-2180-14-53.
11. **Sutherland IW.** 2001. Biofilm exopolysaccharides: a strong and sticky framework. Microbiology **147:**3–9. http://dx.doi.org/10.1099/00221287-147-1-3.
12. **Renault M, Cukkemane A, Baldus M.** 2010. Solid-state NMR spectroscopy on complex biomolecules. Angew Chem Int Ed Engl **49:**8347–8357.
13. **Cegelski L, Hing AW, Kim SJ, Studelska DR, O'Connor RD, Mehta AK, Schaefer J.** 2002. Rotational-echo double resonance characterization of vancomycin mode of action in *S. aureus*. Biochemistry **41:**13053–13058. http://dx.doi.org/10.1021/bi0202326.
14. **Curtis-Fisk J, Spencer RM, Weliky DP.** 2008. Native conformation at specific residues in recombinant inclusion body protein in whole cells determined with solid-state NMR spectroscopy. J Am Chem Soc **130:**12568–12569. http://dx.doi.org/10.1021/ja8039426.
15. **Toke O, Cegelski L.** 2010. REDOR applications in biology: an overview, p 743–490. *In* McDermott AE, Polenova T (ed), Solid-state NMR studies of biopolymers. John Wiley & Sons Ltd., Chichester, United Kingdom.
16. **Kim SJ, Chang J, Singh M.** 2015. Peptidoglycan architecture of Gram-positive bacteria by solid-state NMR. Biochim Biophys Acta Biomembr **1848:**350–362. http://dx.doi.org/10.1016/j.bbamem.2014.05.031.
17. **Yamamoto K, Caporini MA, Im SC, Waskell L, Ramamoorthy A.** 2015. Cellular solid-state NMR investigation of a membrane protein using dynamic nuclear polarization. Biochim Biophys Acta Biomembr **1848:**342–349. http://dx.doi.org/10.1016/j.bbamem.2014.07.008.
18. **Ramamoorthy A.** 2009. Beyond NMR spectra of antimicrobial peptides: dynamical images at atomic resolution and functional insights. Solid State

Nucl Magn Reson **35:**201–207. http://dx.doi.org/10.1016/j.ssnmr.2009.03.003.
19. **Lim JY, May JM, Cegelski L.** 2012. Dimethyl sulfoxide and ethanol elicit increased amyloid biogenesis and amyloid-integrated biofilm formation in *E. coli*. Appl Environ Microbiol **78:**3369–3378. http://dx.doi.org/10.1128/AEM.07743-11.
20. **McCrate OA, Zhou X, Reichhardt C, Cegelski L.** 2013. Sum of the parts: composition and architecture of the bacterial extracellular matrix. J Mol Biol **425:**4286–4294. http://dx.doi.org/10.1016/j.jmb.2013.06.022.
21. **Reichhardt C, Fong JC, Yildiz F, Cegelski L.** 2015. Characterization of the *Vibrio cholerae* extracellular matrix: a top-down solid-state NMR approach. Biochim Biophys Acta **1848:**378–383. http://dx.doi.org/10.1016/j.bbamem.2014.05.030.
22. **Reichhardt C, Cegelski L.** 2014. Solid-state NMR for bacterial biofilms. Mol Phys **112:**887–894. http://dx.doi.org/10.1080/00268976.2013.837983.
23. **Hall-Stoodley L, Costerton JW, Stoodley P.** 2004. Bacterial biofilms: from the natural environment to infectious diseases. Nat Rev Microbiol **2:**95–108. http://dx.doi.org/10.1038/nrmicro821.
24. **Zarnowski R, Westler WM, Lacmbouh GA, Marita JM, Bothe JR, Bernhardt J, Lounes-Hadj Sahraoui A, Fontaine J, Sanchez H, Hatfield RD, Ntambi JM, Nett JE, Mitchell AP, Andes DR.** 2014. Novel entries in a fungal biofilm matrix encyclopedia. mBio **5:**e01333-14. http://dx.doi.org/10.1128/mBio.01333-14.
25. **Oda K, Kakizono D, Yamada O, Iefuji H, Akita O, Iwashita K.** 2006. Proteomic analysis of extracellular proteins from *Aspergillus oryzae* grown under submerged and solid-state culture conditions. Appl Environ Microbiol **72:**3448–3457. http://dx.doi.org/10.1128/AEM.72.5.3448-3457.2006.
26. **Banerjee B, Greenberger PA, Fink JN, Kurup VP.** 1998. Immunological characterization of Asp f 2, a major allergen from *Aspergillus fumigatus* associated with allergic bronchopulmonary aspergillosis. Infect Immun **66:**5175–5182.
27. **Schaefer J, Stejskal EO.** 1976. Carbon-13 nuclear magnetic resonance of polymers spinning at the magic angle. J Am Chem Soc **98:**1031–1032. http://dx.doi.org/10.1021/ja00420a036.
28. **Schaefer J, Stejskal EO, Buchdahl R.** 1975. High-resolution carbon-13 nuclear magnetic resonance study of some solid, glassy polymers. Macromolecules **8:**291–296. http://dx.doi.org/10.1021/ma60045a010.
29. **Fukamizo T, Kramer KJ, Mueller DD, Schaefer J, Garbow J, Jacob GS.** 1986. Analysis of chitin structure by nuclear magnetic resonance spectroscopy and chitinolytic enzyme digestion. Arch Biochem Biophys **249:**15–26. http://dx.doi.org/10.1016/0003-9861(86)90555-2.
30. **Bernard M, Latge JP.** 2001. *Aspergillus fumigatus* cell wall: composition and biosynthesis. Med Mycol **39:**S9–S17.
31. **Gullion T, Schaefer J.** 1989. Rotational-echo double-resonance NMR. J Magn Reson **81:**196–200.
32. **Cegelski L, Rice CV, O'Connor RD, Caruano AL, Tochtrop GP, Cai ZY, Covey DF, Schaefer J.** 2005. Mapping the locations of estradiol and potent neuroprotective analogues in phospholipid bilayers by REDOR. Drug Dev Res **66:**93–102. http://dx.doi.org/10.1002/ddr.20048.
33. **Gravelat FN, Beauvais A, Liu H, Lee MJ, Snarr BD, Chen D, Xu W, Kravtsov I, Hoareau CM, Vanier G, Urb M, Campoli P, Al Abdallah Q, Lehoux M, Chabot JC, Ouimet MC, Baptista SD, Fritz JH, Nierman WC, Latge JP, Mitchell AP, Filler SG, Fontaine T, Sheppard DC.** 2013. *Aspergillus* galactosaminogalactan mediates adherence to host constituents and conceals hyphal beta-glucan from the immune system. PLoS Pathog **9:**e1003575. http://dx.doi.org/10.1371/journal.ppat.1003575.
34. **Loussert C, Schmitt C, Prevost MC, Balloy V, Fadel E, Philippe B, Kauffmann-Lacroix C, Latge JP, Beauvais A.** 2010. In vivo biofilm composition of *Aspergillus fumigatus*. Cell Microbiol **12:**405–410. http://dx.doi.org/10.1111/j.1462-5822.2009.01409.x.
35. **Elkins JG, Hassett DJ, Stewart PS, Schweizer HP, McDermott TR.** 1999. Protective role of catalase in *Pseudomonas aeruginosa* biofilm resistance to hydrogen peroxide. Appl Environ Microbiol **65:**4594–4600.
36. **Miller RA, Britigan BE.** 1997. Role of oxidants in microbial pathophysiology. Clin Microbiol Rev **10:**1–18.
37. **Calera JA, Paris S, Monod M, Hamilton AJ, Debeaupuis J-P, Diaquin M, Lopez-Medrano R, Leal F, Latge J-P.** 1997. Cloning and disruption of the antigenic catalase gene of *Aspergillus fumigatus*. Infect Immun **65:**4718–4724.
38. **Jahn B, Langfelder K, Schneider U, Schindel C, Brakhage AA.** 2002. PKSP-dependent reduction of phagolysosome fusion and intracellular kill of *Aspergillus fumigatus* conidia by human monocyte-derived macrophages. Cell Microbiol **4:**793–803. http://dx.doi.org/10.1046/j.1462-5822.2002.00228.x.
39. **Zhong J, Frases S, Wang H, Casadevall A, Stark RE.** 2008. Following fungal melanin biosynthesis with solid-state NMR: biopolymer molecular structures and possible connections to cell-wall polysaccharides. Biochemistry **47:**4701–4710. http://dx.doi.org/10.1021/bi702093r.
40. **Banerjee A, Supakar S, Banerjee R.** 2014. Melanin from the nitrogen-fixing bacterium *Azotobacter chroococcum*: a spectroscopic characterization. PLoS One **9:**e84574. http://dx.doi.org/10.1371/journal.pone.0084574.
41. **Rajendran R, Williams C, Lappin DF, Millington O, Martins M, Ramage G.** 2013. Extracellular DNA release acts as an antifungal resistance mechanism in mature *Aspergillus fumigatus* biofilms. Eukaryot Cell **12:**420–429. http://dx.doi.org/10.1128/EC.00287-12.